Available online at www.sciencedirect.com

ScienceDirect

materialstoday: PROCEEDINGS

Materials Today: Proceedings 2 (2015) 474 – 482

12th European Conference on Thermoelectrics

Explicitly accounting for the heat sink strengths in the thermal matching of thermoelectric devices. A unified practical approach

Dario Narducci*

University of Milano Bicocca, Dept. Materials Science, via R. Cozzi 55, 20125 Milano, Italy

Abstract

Thermal matching of thermoelectric generators (TEGs) to their heat sinks is well known to be a critical issue in the development of efficient harvesters. It is slightly less obvious that the development of suitable novel materials would possibly take advantage of their contextualization to prospective scenarios of deployment. In this communication a novel unified analysis of the heat equation is proposed. The thermal system was embedded into a thermostat while the heat source was taken as a part of the system itself, also explicitly accounting for the heat dissipation. A continual transition of thermal matching conditions from those predicted under Dirichlet boundary conditions (BCs) to those obtained under Neumann BCs was found, depending on the strength of the heat source and on the thermal resistances of the circuit branches. In all cases it was found that, independently of the thermal or thermoelectric circuit geometry, no single material may provide optimal TEG power density for any heat source strength and branch resistance.

Selection and peer-review under responsibility of Conference Committee members of the 12th European Conference on Thermoelectrics.

Keywords: Thermoelectricity. Thermoelectric generators, Thermal matching

1. Introduction

Thermal matching of thermoelectric generators (TEGs) to their heat sinks is a well assessed issue in the making of efficient harvesting systems. Beyond a proper choice of the thermoelectric (TE) material, capable of providing the

* Corresponding author. Tel.: +39-02-64485137; fax: +39-02-64485400.
E-mail address: dario.narducci@unimib.it

Selection and peer-review under responsibility of Conference Committee members of the 12th European Conference on Thermoelectrics.
doi:10.1016/j.matpr.2015.05.065

highest conversion efficiency in the relevant temperature range, TEGs should also optimize their heat flow acceptance while keeping the temperature drop across the TE element as large as possible. For any given thermoelectric efficiency, exceedingly low thermal conductances lead actually to reduced thermal currents, and therefore to low electrical power densities [1, 2]; while high thermal conductances for finite thermal power inputs may cause low temperature differences between hot and cold sides of TE elements. To make the scenario even more complicated, optimal TEG design critically depends upon the assumptions made about the operative conditions the TEG will operate in, namely whether heat sink temperatures or heat flow can be taken as fixed.

Aim of this paper is to propose a general approach to thermal matching in TEGs that overcomes any arbitrary assumption about boundary conditions (BCs) at TEG ends. In order to do that, a general scheme will be proposed embedding the heat sinks within the system to be analyzed. The entire system is then put in contact with the ambient, and the heat flow through dissipators may be analyzed by safely assuming that the ambient acts as a thermal bath. In this approach it will be shown how, further to TEG, heat sink thermal resistances and dissipaters, also the heat source strength plays a major role in the design of the harvesting devices. These results will be shown to be especially critical under two circumstances, namely when nanostructured TE elements (e.g. nanowires and nanolayers) are used or when TEGs are meant as microharvesters, converting heat from low thermal power sources.

2. Model

The maximum electric power w generated by a TE element operating between two heat sinks at T_H and T_C ($< T_H$) is $w = \dot{Q}\eta$, where η is the thermoelectric efficiency

$$\eta = \frac{\Delta T}{T_H}\frac{\beta - 1}{\beta + T_H / T_C} \tag{1}$$

$\Delta T = T_H - T_C$ is the temperature difference across the TE element, $\beta = \sqrt{1 + Z\overline{T}}$ with $\overline{T} = (T_H + T_C)/2$, and the thermoelectric figure of merit ZT equals $\alpha^2 \sigma T / \kappa = \alpha^2 T / (RG_{th})$ (where σ and κ are respectively the electrical and thermal conductivities of the TE material, α is the Seebeck coefficient, and R and G_{th} are the TE electric and thermal conductances). Furthermore, the heat current $\dot{Q}$ through the TE element is proportional to its thermal conductance, namely $\dot{Q} = G_{th}\Delta T$.

Under constant heat flow BCs (fixed $\dot{Q}$), both $\Delta T = \dot{Q} / G_{th}$ and therefore the thermodynamic TE efficiency increase with vanishing G_{th}. Accordingly, also w increases as G_{th} decreases, up to reaching $\dot{Q}$ for unitary efficiency when ΔT diverges. Then, for any given TE material, optimal w is expected for low thermal conductances, namely for long TE legs and/or small TE cross sections. Instead, when fixed–temperature BCs are set, $\dot{Q}$ and w are larger for larger G_{th}, namely $w \to \infty$ for $G_{th} \to \infty$. In this case, optimal power output seemingly calls for large G_{th} values, suggesting short TE legs and/or large TE cross sections [3]. These well known, apparently paradoxical conclusions solve out considering that in no real circumstance do constant temperature (Dirichlet) or constant heat flow (Neumann) BCs strictly hold. Stated differently, neither real heat power sinks can guarantee fixed boundary temperatures for arbitrarily large thermal conductance, nor can they provide constant heat currents for extremely small G_{th}. However, solving the heat equation without such BCs is rather cumbersome, and the search for a transitional solution covering intermediate and more realistic operational conditions has led to iterative self–consistent approaches [3, 4].

A more general, possibly more rigorous approach to the problem is schematised in Fig. 1 for a pseudo–one–dimensional system. The basic idea is to replace the standard picture, where the pertinent heat equation is solved setting system boundaries at the ends of the TE device, with a representation where the TEG and the two heat baths are embedded into the system. As a result, system boundaries are in thermal contacts with a heat sink of infinite thermal capacity (the ambient), capable of guaranteeing constant temperature BCs under any circumstance.

Under steady state conditions heat equation reverts to Poisson's equation [5], namely $\kappa T''(x) + q(x) = 0$ where $q(x)$ is the thermal power strength density. For a point source of strength Ω (in W/m^3) located at x_0 it is $q(x) = \Omega\delta(x - x_0)$ (where $\delta(x)$ is the Dirac delta function). Taking instead a uniform heat generation along a segment of length d centred at x_0 one may write

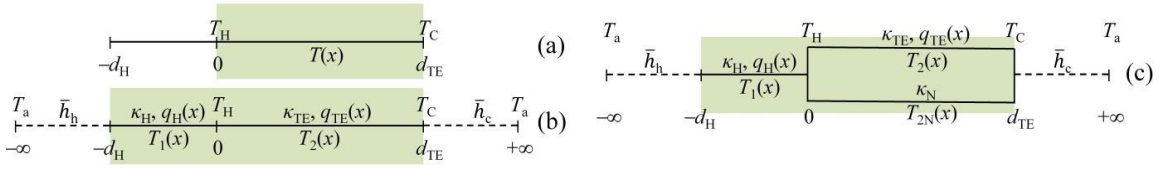

Figure 1. Schematics of (a) the conventional, (b) the non-shunted and (c) the shunted sink-embedding representation of a uni-leg TEG. Colored areas mark the actual extension of the systems. The standard model assumes either fixed boundary temperatures or fixed heat flow through the thermoelectric leg. In the present model the heat source is instead considered as a part of the system, so that no arbitrary assumption is needed about BCs at TEG ends, while Dirichlet BCs apply to the overall system (TEG + heat source + dissipaters).

$$q(x) = \frac{Q}{d}\Pi\left(\frac{x - \frac{1}{2}x_0}{d}\right) \tag{2}$$

where Q is the strength of a linear heat source (in W/m^2) while $\Pi(z)$ is the normalized boxcar function:

$$\Pi(z) = \begin{cases} 1 & \text{for } -\frac{1}{2} \le z \le -\frac{1}{2} \\ 0 & \text{otherwise} \end{cases} \tag{3}$$

that integrates to

$$\int_{-\infty}^{+\infty} q(x)\mathrm{d}x = Q \tag{4}$$

Heat dissipation at system boundaries is described using the so–called Newton's law of cooling, namely scaling the heat current with temperature at the (convective) dissipaters as $\bar{h}(T - T_a)$, where $\bar{h}$ is the heat transfer coefficient (in Wm^{-2}K^{-1}) and T_a is the ambient temperature. Thus the system is completely described by the following set of ordinary differential equations:

$$\begin{cases} \kappa_{TE} T_2''(x) + q_{TE}(x) = 0 \\ \bar{h}_c (T_2(d_{TE}) - T_A) = -\kappa_{TE} T_2'(d_{TE}) \\ \kappa_H T_1''(x) + q_H(x) = 0 \\ \bar{h}_h (T_1(-d_H) - T_A) = \kappa_H T_1'(-d_H) \\ \kappa_{TE} T_2'(0) = \kappa_H T_1'(0) \\ T_1(0) = T_2(0) \end{cases} \tag{5}$$

where d_{TE} and d_H are the leg and the hot sink lengths, κ_{TE} and κ_H their thermal conductivities, and $\bar{h}_h$ and $\bar{h}_c$ are the heat transfer coefficients of the dissipaters at the hot and cold sides of the system [6]. Note that the Eq. (5) refers to a one-dimensional system, thus all extensive quantities are normalized to a sectional area. A heat source of power density $q_H(x) > 0$ and a heat sink of power density $q_{TE}(x) < 0$ are embedded in the system, representing respectively the thermal power source and the sum of the heat converted by the TEG into electric energy and other heat losses (*e.g.* lateral heat dissipation). Finally, temperature profiles are conveniently described by two different functions, $T_1(x)$ and $T_2(x)$, with domains respectively for $x < 0$ (thermal source) and $x > 0$ (TE leg).

In spite of the seeming simplicity of Eqs. (5), their analytical solution is rather cumbersome. To make it more physically readable it may be convenient to cast Eqs. (5) into a dimensionless form. To this aim, the reduced coordinate $\hat{x} \equiv x / d_{\mathrm{TE}}$ and two reduced temperatures $v_i \equiv T_i / T_{\mathrm{a}} - 1\,(i = 1, 2)$ are introduced. Setting

$$\begin{aligned} q_{\mathrm{H}}(x) &\equiv \frac{\theta_{\mathrm{H}}}{d_{\mathrm{H}}}\Pi\left(\frac{x}{d_{\mathrm{H}}} + \frac{1}{2}\right) > 0 \\ q_{\mathrm{TE}}(x) &\equiv -\frac{\theta_{\mathrm{TE}}}{d_{\mathrm{TE}}}\Pi\left(\frac{x}{d_{\mathrm{TE}}} - \frac{1}{2}\right) < 0 \end{aligned} \tag{6}$$

and with some manipulations Eqs. (5) can be rewritten as

$$\begin{cases} v_2''(\hat{x}) = \mu_3\Pi(\hat{x} - \frac{1}{2}) \\ v_2(1) = -\mu_5 v_2'(1) \\ v_1''(\hat{x}) = -\mu_2\mu_1^{-2}\Pi\left(\hat{x}\mu_1^{-1} + \frac{1}{2}\right) \\ v_1(-\mu_1) = \mu_4\mu_1 v'_1(-\mu_1) \\ v_1'(0) = \mu_6 v_2'(0) \\ v_1(0) = v_2(0) \end{cases} \tag{7}$$

Table 1 displays the definitions of the dimensionless parameters in Eqs. (7) along with typical values of both dimensioned and dimensionless parameters. Furthermore, one may define $\tilde{z} \equiv ZT_{\mathrm{a}}$ and a dimensionless heat current $\tilde{\phi} \equiv \phi / \theta_{\mathrm{H}}$. Thus, the reduced electric power output reads $\tilde{w} \equiv w / \theta_{\mathrm{H}}$.

Solving the heat equation returns second–degree polynomials for v_1 and v_2, namely

$$v_i(\hat{x}) = \sum_{j=0}^{2} (\beta_{ji} / \beta_D)\hat{x}^j \tag{8}$$

with

$$\begin{aligned} \beta_{02} &= \mu_2(1+2\mu_4)(1+\mu_5) - \mu_1\mu_3\mu_6(1+\mu_4)(1+2\mu_5) & \beta_{01} &= \beta_{02} \\ \beta_{12} &= -(\mu_2(1+2\mu_4) + \mu_3(1+2\mu_5)) & \beta_{11} &= -\mu_6(\mu_2(1+2\mu_4) + \mu_3(1+2\mu_5)) \\ \beta_{22} &= \frac{\mu_3\beta_{\mathrm{D}}}{2} & \beta_{21} &= -\frac{\mu_2}{2\mu_1^2}\beta_{\mathrm{D}} \end{aligned} \tag{9}$$

and $\beta_{\mathrm{D}} = 2\left(1 + \mu_5 + \mu_1\mu_6\left(1 + \mu_4\right)\right)$. The temperature at the leg ends computes therefore to

$$v_{\mathrm{h}} \equiv v_2(0) = \beta_{02} / \beta_D, \quad v_{\mathrm{c}} \equiv v_2(1) = \sum_{j=0}^{2} \beta_{j2} / \beta_D \tag{10}$$

The heat flow (heat current) at $\hat{x} = 0$ immediately follows:

$$\tilde{\phi} = -\frac{\mu_1\mu_6}{\mu_3}\frac{\beta_{12}}{\beta_{\mathrm{D}}} \tag{11}$$

Table 1. Physical quantities and dimensionless parameters used in the model Eqs. (5) and (7), and range of values relevant to microharvesting applications.

Quantity	Units	Range of values	Parameter	Definition	Range of values
κ_H, κ_{TE}	$Wm^{-1}K^{-1}$	$[10^{-1}, 10^{2}]$	μ_1	d_H/d_{TE}	$[10^{-1}, 10^{6}]$
$\bar{h}_h$, $\bar{h}_c$	$Wm^{-2}K^{-1}$	$[10^{-1}, 10^{3}]$	μ_2	$\theta_H d_H/(T_a\kappa_H)$	$[3\times10^{-8}, 3\times10^{2}]$
θ_H	Wm^{-2}	$[1, 10^{5}]$	μ_3	$\theta_{TE} d_{TE}/(T_a\kappa_{TE})$	$[3\times10^{-14}, 3]$
θ_{TE}	Wm^{-2}	$[10^{-2}, 10^{4}]$	μ_4	$\kappa_H / (d_H \bar{h}_h)$	$[10^{-3}, 10^{6}]$
d_H	m	$[10^{-3}, 10^{-1}]$	μ_5	$\kappa_{TE} / (d_{TE} \bar{h}_c)$	$[10^{-2}, 10^{10}]$
d_{TE}	m	$[10^{-7}, 10^{-2}]$	μ_6	κ_{TE}/κ_H	$[10^{-3}, 10^{3}]$

Explicit expressions could also be written for the thermoelectric efficiency η and for the dimensionless power output $\tilde{w}$. However, they are very clumsy and will not be reported. Instead, special cases of interest for the actual optimization of TEGs will be commented upon in the next Section.

3. Results

3.1. Dirichlet and Neumann limits

First, let us reconcile the results of the model with standard solutions of the heat equation under Dirichlet and Neumann BCs. For a highly dissipating cold side and a properly insulated hot side ($1/\mu_4 = 0$, $\mu_5 = 0$), taking $\kappa_{TE} = \kappa_H$ = 10 W/mK and $\theta_H = 10^4$ W/m^2 the hot temperature side ranges from T_a = 300 K to about 700 K ($\Delta v \equiv v_h - v_c \approx 1$) for large μ_1 ($\geqslant 1$). Instead, $\tilde{\phi}$ displays a constant value (variations smaller than 10^{-5}) close to unity, as one would expect under fixed heat flow BCs (Fig. 2). A perfect quantitative agreement is thus found comparing solutions of Eqs. (7) to the standard solution of the heat equation under Neumann conditions. In the opposite limit (small μ_1) the general solution is better approximated by the standard solution under Dirichlet conditions – namely the heat flow linearly decreases with d_{TE} while the temperature drop across the TE leg remains constant.

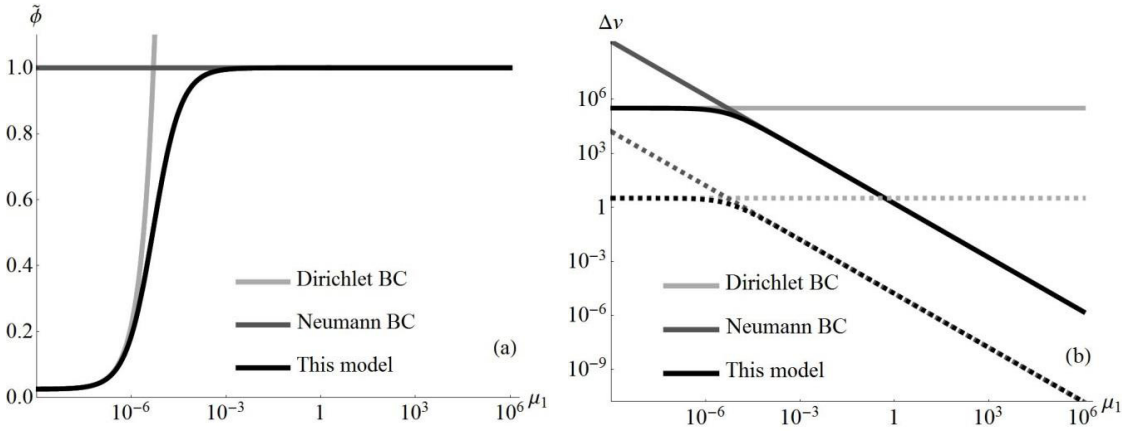

Figure 2: Dependency of (a) $\tilde{\phi}$ and (b) $\Delta v \equiv v_h - v_c$ upon μ_1 compared to standard solutions of the heat equation under Neumann and Dirichlet conditions. Plots assume a highly dissipating cold side ($\bar{h}_c = 10^3$ Wm^{-2}K^{-1}) and a properly insulated hot side ($\bar{h}_h = 10^{-3}$ Wm^{-2}K^{-1}) and $\kappa_{TE} = \kappa_H$ = 10 Wm^{-1}K^{-1}. Two thermal power densities are considered, namely $\theta_H = 10^5$ Wm^{-2} (full lines) and $\theta_H = 1$ Wm^{-2} (dashed lines). Note that the dimensionless thermal current $\tilde{\phi}$ is independent of θ_H.

It is worth noting that for realistic values of μ_1 Neumann BCs apparently well describe the heat transport regime. This is not surprising in view of the stipulations about heat dissipation at system boundaries. This picture quite changes when dissipation is less than ideal. Actually, heat sources less thermally insulated toward the ambient lead to deviations of $\tilde{\phi}(\mu_1)$ from constant values even at relatively high μ_1 values. Correspondingly, the temperature drop across the TE leg departs from its linear trend, approaching an asymptotic limit (Fig. 3).

This is consistent with a lower thermal current flowing from the source through the TE element. The very same result is obtained by decreasing θ_{TE} (q_{TE}) — while instead only marginal changes in the $\tilde{\phi}(\mu_1)$ plot are observed by changing $\bar{h}_c$ (not shown). This evidence further underlines how in a relevant region of the μ–space neither Dirichlet or Neumann BCs properly describe heat conduction in TEGs.

3.2. Optimization of power output

Manifestly enough, optimal power generation geometries occur when a convenient compromise between heat flow maximization and high conversion efficiency is found. Under ideal dissipation conditions (namely perfect insulation at $\hat{x} = -1$, *i.e.* $1/\mu_4 = 0$; and perfect heat dissipation at $\hat{x} = 1$, *i.e.* $\mu_5 = 0$) the heat current accounts to $\tilde{\varphi} = \mu_2 / (\mu_1 \mu_3 \mu_6)$ while the conversion efficiency reads

$$\eta = \frac{(\psi - 2)(\mu_1 \mu_3 \mu_6 - 2\mu_2)}{-4\mu_1 \mu_6 + \psi(\mu_1 \mu_6 (\mu_3 - 2) - 2\mu_2)} \tag{12}$$

and the reduced power output simplifies to

$$\tilde{w} = \frac{\mu_2 (\psi - 2)(\mu_1 \mu_3 \mu_6 - 2\mu_2)}{\mu_1 \mu_3 \mu_6 [\psi(\mu_1 \mu_6 (\mu_3 - 2)) - 4\mu_1 \mu_6]} \tag{13}$$

where $\psi \equiv \sqrt{4 + \tilde{z}(4 - \mu_3 + 2\tilde{z}\mu_2 \mu_1^{-1} \mu_6^{-1})}$. One easily verifies that $\eta \to 1$ for $\mu_1 \to 0$. Actually, for $d_{TE} \to \infty$ the thermal resistance of the TE leg diverges so that for any non–zero thermal current the temperature drop across the TE also diverges. Since it has been shown that ideally dissipating systems may be properly modeled as if Neumann BC held, one may correspondingly expect power output to increase with the TE leg length. This is actually the case in the range of practical interest for microharvesting, where $\tilde{w}$ rapidly increases for vanishing μ_1 values (Fig. 4(a)).

For sub–ideal heat source insulation one observes instead (Fig. 4(b)) that the power output is basically independent of μ_1 for low μ_1 values. This finds a simple interpretation considering that for large leg lengths (high TE thermal resistances) the conversion efficiency reaches a plateau while some of the thermal power finds a lower impedance route at the outer heat source well. Thus, the heat current flowing through the TE leg cannot indefinitely increase. For higher μ_1, instead, dissipation at $\hat{x} = -1$ becomes less important and $\tilde{w}$ increases as in the ideal case. Since Δv levels up in the same μ_1 range where dissipation of the hot source toward the ambient begins affecting the heat flow through the TE leg, a small inflection of the output power occurs upon transition between the regimes of constant and increasing power output.

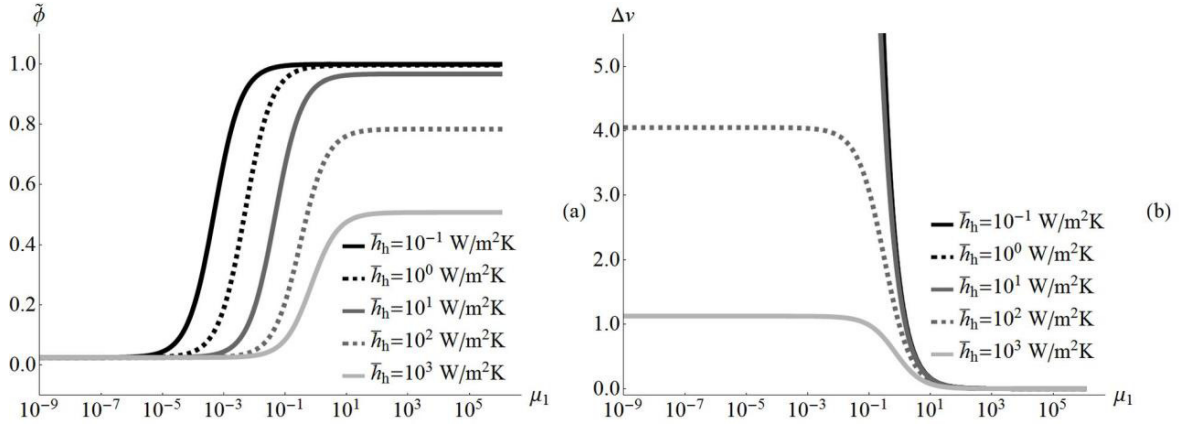

Figure 3: Dependency of (a) $\tilde{\phi}$ and (b) $\Delta v \equiv v_h - v_c$ upon μ_1 at different levels of thermal insulation of the hot source, with a highly dissipating cold side ($\bar{h}_c = 10^3$ Wm^{-2}K^{-1}). Thermal conductivities and thermal power densities are $\kappa_{TE} = \kappa_H = 10$ Wm^{-1}K^{-1}, and $\theta_H = 10^5$ Wm^{-2}.

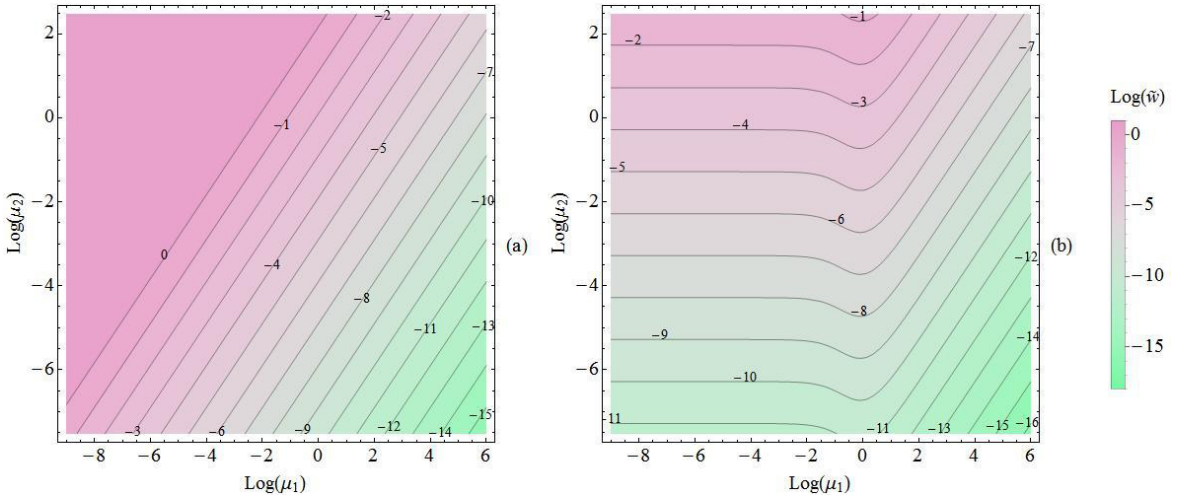

Figure 4. Variation of the dimensionless power output with $\mu_1$and μ_2 under (a) ideal insulation of the heat source ($1/\mu_4 = 0$) or (b) sub--ideal insulation ($\mu_4 = 10^{-2}$). Heat dissipation on the cold end of the TE element is assumed as ideal ($\mu_5 = 0$). Thermal conductivities of the TE element and of the heat source are taken equal to each other ($\mu_6 = 1$).

3.3. Thermal shunts

In real systems, heat flow shunts normally occur through air (in bulk TEGs) or through the substrate (in thin film or nanostructured TEGs) – and through the TEG package as well. Shunts can be easily accounted for in the present model. Forking the thermal circuit between $x = 0$ and $x = d_{TE}$ (Fig. 1(c)) into thermoelectrically active and non–thermoelectrically active branches (hereafter referred to as T– and N–branches, resp.), heat equation for the shunted system may be obtained by adding to Eqs. (5)

$$\begin{aligned} \kappa_N T_{2N}''(x) &= 0 \\ T_2(0) &= T_{2N}(0) \end{aligned} \tag{14}$$

and replacing the fifth of Eqs. (5) with

$$\kappa_H T_1'(0) = \kappa_{TE} T_2'(0) + \kappa_N T_{2N}'(0) \tag{15}$$

where $T_{2N}(x)$ is the temperature profile over the N – branch and κ_N is its thermal conductivity. Reduced variables may be defined also in this case, leading to the additional parameter $\mu_7 \equiv \kappa_N/\kappa_H$. The dimensionless equation reads then

$$\begin{cases} v_2''(\hat{x}) = \mu_3 \Pi(\hat{x} - \frac{1}{2}) & v_1(0) = v_2(0) \\ v_2(1) = -\mu_5 v_2'(1) - \mu_5 \mu_7 \mu_6^{-1} v_{2N}'(1) & v_{2N}''(0) = 0 \\ v_1''(\hat{x}) = -\mu_2 \mu_1^{-2} \Pi\left(\hat{x}\mu_1^{-1} + \frac{1}{2}\right) & v_2(0) = v_{2N}(0) \\ v_1(-\mu_1) = \mu_4 \mu_1 v'_1(-\mu_1) & v_2(1) = v_{2N}(1) \\ v_1'(0) = \mu_6 v_2'(0) + \mu_7 v_{2N}'(0) & \end{cases} \tag{16}$$

where $v_{2N}(\hat{x}) \equiv T_{2N}/T_a - 1$. It integrates to give

$$\Delta v = \frac{\mu_5\left(\mu_2\left(2\mu_4+1\right)\left(\mu_6+\mu_7\right) - \mu_3\mu_6\left(2\mu_1\left(\mu_4+1\right)\left(\mu_6+\mu_7\right)+1\right)\right)}{2\mu_6\left(\mu_5+\mu_1\left(\mu_4+1\right)\mu_6+1\right)+2\left(\mu_5+\mu_1\left(\mu_4+1\right)\mu_6\right)\mu_7} \tag{17}$$

while

$$\tilde{\phi} = \frac{\mu_2\left(2\mu_4+1\right)\left(\mu_6+\mu_7\right)+\mu_3\left(\left(2\mu_5+1\right)\mu_6+2\mu_5\mu_7\right)}{2\mu_3\left(\mu_6\left(\mu_5+\mu_1\left(\mu_4+1\right)\mu_6+1\right)+\left(\mu_5+\mu_1\left(\mu_4+1\right)\mu_6\right)\mu_7\right)} \tag{18}$$

Eqs. (17) and (18) obviously reduce to Eqs. (10) and (11) for $\mu_7 = 0$. A full analysis of the shunted system exceeds the aims of this paper. Suffice here to say that in the Dirichlet and Neumann limits one may easily verify that also in the presence of a shunt the solution recovers the standard solution for fixed–temperature and fixed–heat flow BCs.

4. Discussion and Conclusions

The numerical results obtained through the model may be of guidance to design thermoelectric generators, either bulk TEGs and nanostructured devices. From inspection of Fig. 4 one clearly realizes the already well–assessed role played by thermal dissipation not only to guarantee steady and efficient heat conversion – but also to properly size the device leg. Specifically, for any given heat dissipation efficiency on the cold side one may compute the optimal leg length by maximizing the power output. The optimal d_{TE} is found to depend on the heat strength of the hot sink as well as on its thermal insulation toward the ambient. This is especially important for nanostructured devices (*e.g.* nanowires), where the design of long and continuous TE element is rather critical. For harvesting applications relying upon small–budgeted heat sources (*e.g.* for body heat harvesting), oversized elements are of no use unless excellent heat dissipation can be guaranteed. In extreme situations where large μ_2 values are reached, relatively shorter TE legs may paradoxically provide larger power outputs. But also in more conventional situations, no advantage is achieved by increasing d_{TE} as the achievable power density levels up. More in general, a conclusion

one may draw is that optimal device design depends not only on the characteristics of the heat dissipator but is also remarkably subjected upon the heat source strength and geometry. This shows once again that, stepping from device physics to material characteristics, optimal TEG design suggest to tailor TE material properties not only in view of high thermoelectric efficiency (high *ZT*) but also considering the more complicated interplay between efficiency and thermal conductivity.

The present analysis, while indirectly covering also non–one–dimensional issues such as lateral dissipation and thermal shunts, does not allow to take apart the heat sink associated to thermoelectric conversion from heat current leaks correlated to device packaging. Splitting q_{TE} requires the solution of the Domenicali equation [7], that is currently under way and that will be reported in a forthcoming article.

Acknowledgements

This work was supported by FP7–NMP–2013–SMALL–7, SiNERGY (Silicon Friendly Materials and Device Solutions for Microenergy Applications) Project, Contract n. 604169.

References

[1] D. Narducci, J. Nanoeng. Nanomanuf. 1 (2011) 63−70.
[2] D. Narducci, Appl. Phys. Lett. 99 (2011) 102104.
[3] V. Leonov, P. Fiorini, and R. J. Vullers, Microelectr. J. 42 (2011) 579−584.
[4] V. Leonov, P. Fiorini, Proc. 5th Eur. Conf. Thermoelectrics, (2007), pp. 129–133.
[5] H. Carslaw, J. Jaeger, Conduction of Heat in Solids, second ed., Oxford Science Publications, Clarendon Press, Oxford,1986.
[6] J. Lienhard, J. Lienhard, A Heat Transfer Textbook, third ed., Dover Publications, Mineola, 2011, pp. 19−21.
[7] C. A. Domenicali, J. Appl. Phys. 25 (1954) 1310−1311.